Carbon nanofibre microfiltration membranes tailored by oxygen plasma for electrocatalytic wastewater treatment in cross-flow reactors

Ahmed O. Rashed[a*], Chi Huynh[b], Andrea Merenda[c], Si Qin[a], Maxime Maghe[d], Lingxue Kong[a], Takeshi Kondo[b], Ludovic F. Dumée[e,f,g*] and Joselito M. Razal[a*]

Affiliations

[a]Deakin University, Geelong, Institute for Frontier Materials, 3216 Waurn Ponds, Victoria, Australia.

[b]LINTEC OF AMERICA, INC. Nano-Science and Technology Center, 2900 E. Plano Pkwy. Suite 100, Plano, Texas 75074, United States of America

[c]School of Science, RMIT University, 124 La Trobe Street, Melbourne, Victoria 3000, Australia

[d]Carbon Nexus, Institute for Frontier Materials, Deakin University, Waurn Ponds, VIC 3216, Australia

[e]Khalifa University, Department of Chemical Engineering, Abu Dhabi, United Arab Emirates

[f]Research and Innovation Center on CO_2 and Hydrogen, Khalifa University, Abu Dhabi, United Arab Emirates

[g]Center for Membrane and Advanced Water Technology, Khalifa University, Abu Dhabi, United Arab Emirates

Corresponding authors

joselito.razal@deakin.edu.au; ludovic.dumee@ku.ac.ae; arashed@deakin.edu.au

Abstract

The engineering of electrocatalytic membrane reactors provides potential perspectives to integrate membrane separation with electrocatalytic technology for efficient removal of emerging organic pollutants from wastewater. Here, electro-responsive microfiltration (MF) carbon nanofibre (CNF) membranes were synthesised by poly(acrylonitrile) PAN electrospinning and subsequent carbonization, followed by oxygen plasma treatment to induce their surface wettability and reactivity for electrocatalytic water treatment. The electrocatalytic performance of CNF membranes was fine-tuned via oxygen plasma treatment to yield reaction kinetic constants up to 29.6×10^{-3} and 15.6×10^{-3} min^{-1} against methylene blue (MB) and acetaminophen (ACP), respectively, which were 1.4 to 1.8 times higher than that exhibited by pristine CNF membranes. The water permeance across CNF membrane was gradually enhanced with increasing the plasma exposure time up to 5 min to exhibit 4.65×10^{3} $L.m^{-2}.h^{-1}.bar^{-1}$, while the removal efficiency of MB and ACP was significantly improved to reach 99 and 91%, respectively during combined MF and EC reaction, which was 2.4 to 10.3 times higher than that achieved during MF alone. The achieved performance of oxygen plasma treated CNF membranes was attributed to their enhanced wettability (water contact angle ~ 24°) and raised electro-oxidation capacity (oxygen evolution potential ~ 1.6 V) with introducing oxygen-containing groups on the membrane surface. This work offers an effective scalable fabrication methodology to engineer flexible and functional CNF membranes with excellent electrocatalytic performance towards cost-effective water treatment.

Keywords

Carbon nanofibres; microfiltration membranes; plasma modification; membrane wettability; electrocatalytic membrane reactors

Graphical abstract

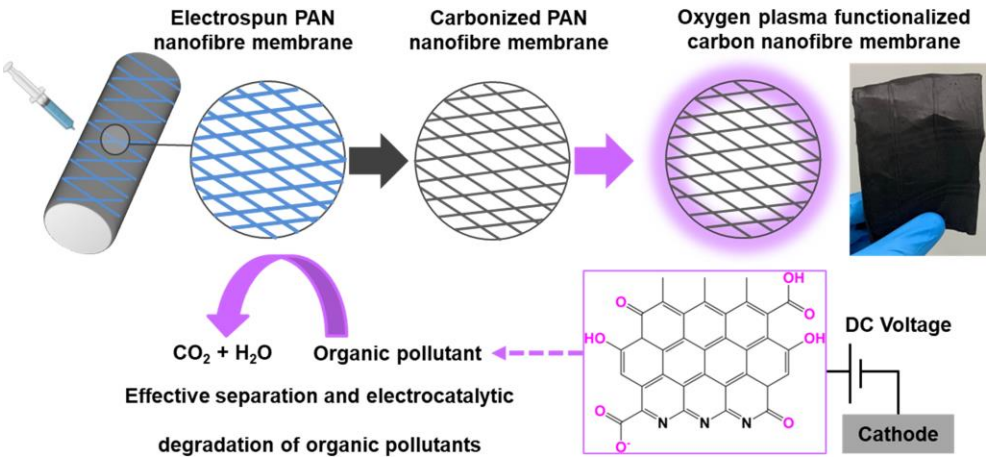

1. Introduction

The growing occurrence of emerging organic pollutants, such as organic dyes, pharmaceutical drugs, and personal care products in water and wastewater have threatened human health and aquatic ecosystems [1-4]. Water remediation methods to tackle this issue were developed based on physical adsorption [5], biological treatment [6], chemical/catalytic oxidation [7], and membrane separation [8]. Membrane technologies, such as microfiltration (MF) and ultrafiltration (UF) have been widely employed in the remediation of water and wastewater due to their operation simplicity, relatively low cost, and high separation efficiency [9-12]. However, both MF and UF are limited by the membrane fouling issue due to the accumulation of the captured organic pollutants on the surface or pores of the membranes, leading to water permeability decline [13-15].

Electrocatalytic membrane reactors (ECMRs) were developed as hybrid water treatment technologies to overcome the latter challenges by integrating membrane separation with electrocatalytic degradation of organic pollutants [16-18]. In ECMRs, the generated oxidizing radicals and electron transfer are the main mechanisms for the degradation of organic pollutants by applying a potential difference between electro-conductive membrane anode and cathode, enhancing mass transfer from the bulk solution to the reactive membrane anode surface during the membrane filtration process [19, 20]. To date, membrane electrode materials involve mainly inorganic ceramic, polymer composite and carbon-based membranes [21]. Inorganic ceramic membranes were frequently employed in ECMRs due to their high electrocatalytic performance towards organic pollutant remediation [17, 22]. For example, mixed Ti_4O_7 and Ti_5O_9 membranes were found to degrade 79% of acetaminophen pharmaceutical with a reaction kinetic constant of 17.3×10^{-3} min^{-1} at an applied cell voltage of 4 to 6.5 V [23]. However, the fabrication of ceramic

ECMRs requires complex chemical and thermal treatment methods, while metal/metal oxide materials can be exposed to corrosion and leaching during the electrocatalytic reactions [24-27]. In contrast, polymer composite membrane anodes were fabricated by incorporating conductive nanomaterials within the polymeric matrices via wet chemistry or deposition techniques to improve their electrical conductivity and electrocatalytic properties. For instance, ZnO coated electrospun poly(acrylonitrile) (PAN) membranes were found to achieve excellent removal efficiency above 95% against various organic dyes with a reaction kinetic constant of 4.9×10^{-3} min^{-1} after the application of 15 to 30 V [13]. Nonetheless, polymer composite membranes were limited by their poor electrical conductivity and reduced electrocatalytic performance [28].

On the other hand, carbon-based membranes have captured a great interest in the development of ECMRs due to their high electrical conductivity, excellent adsorption capability and mechanical stability [29]. Recently, PAN-based carbon nanofibres were reported as promising candidates to develop microfiltration ECMRs due to their large specific surface area, high electrical conductivity, and low cost [30-32]. The electrospinning of PAN dope solutions has become a versatile technique to synthesize continuous porous carbon nanofibre (CNF) membranes via thermal stabilization and carbonization of electrospun PAN membranes [30, 33, 34]. However, the electrospun PAN-based CNF membranes were found to suffer from poor mechanical properties, limited wettability, and reduced electro-oxidation capacity due to the lack of active functional groups on CNF membrane surface [29, 30]. Considerable effort has been expended to improve the wettability and electrochemical properties of CNF membranes by chemical functionalization with metal/metal oxide nanomaterials [30, 35]. For example, SnO_2 incorporated CNF membranes incorporated were found to remove 85% of sulfamethoxazole during combined microfiltration and electrocatalytic (MF/EC) reaction with a reaction kinetic constant of $3.9 \times 10^{-}$

^{3} min^{-1} at an applied cell voltage of only 1 V [30]. CNF membranes were also coated with Fe/Co alloy nanoparticles and found to degrade 100% of tetracycline during combined MF/EC reaction with a reaction kinetic constant of 9.5×10^{-3} min^{-1} [35]. However, the latter functionalization methods involve complicated wet chemistry and hydrothermal treatment that limit their feasibility. Conversely, oxygen plasma treatment was suggested as an innovative clean technology to introduce oxygen-containing groups on carbon materials without using any chemicals or solvents to improve their wettability and surface reactivity [29, 36, 37]. The physicochemical and electrochemical properties of carbon materials can be fine-tuned by manipulating the parameters of plasma treatment, opening possibilities for CNF membranes in electrocatalytic water treatment. Therefore, it is worth investigating the impact of oxygen plasma treatment on the separation and electrocatalytic performance of electrospun CNF membranes towards a scaled-up fabrication of reactive ECMRs from carbon nanofibres.

Here, a novel approach to synthesize hydrophilic flexible CNF microfiltration membranes was proposed using PAN electrospinning and carbonization, followed by oxygen plasma treatment. Through oxygen plasma treatment, the wettability and reactivity of CNF membranes were improved, enabling favourable contact between the CNF reactive sites and the aqueous electrolytic solutions. Thus, the synthesized oxygen plasma treated CNF membranes can provide effective platforms for simultaneous separation and electrocatalytic degradation of multiple organic pollutants in cross-flow membrane reactors. The expansion of such innovative electrocatalytic CNF membranes will enable feasible manufacturing of ECMRs with controllable surface reactivity and distinctive electrocatalytic performance via oxygen plasma treatment to support the expansion of water remediation systems.

2. Materials and methods

2.1. Materials

Copolymerized poly(acrylonitrile) (PAN) precursors with 1 wt.% itaconic acid and 3 wt.% methyl methacrylate were obtained from (Jilin Tanggu, China). N,N-dimethylformamide (DMF) (analytical reagent, 99.8%) was purchased from (Chem-Supply, Australia). Sodium sulfate (Na_2SO_4) (anhydrous, ≥99.0%), methylene blue (MB) dye (hydrated, >99.5%), and acetaminophen (ACP) pharmaceutical (≥99.0%) and were purchased from Sigma-Aldrich.

2.2. Fabrication of nanofibrous PAN membranes

The nanofibrous PAN membranes were synthesized using electrospinning technique as previously reported [34]. Briefly, dope solutions of 5 to 12 wt.% PAN in DMF were prepared by stirring at room temperature until homogenous solutions were obtained. Dissolved PAN/DMF solutions were filled into 20 mL plastic syringes connected to (23 Gauge) metal needles. The syringes were then fixed in a commercial electrospinning system (HOLMARC HO-NFES-043 U, Kerala, India). The electrospinning parameters were fixed at an applied voltage of 20 KV and a flow rate of 0.8 $mL.h^{-1}$. The electrospun nanofibres were collected on a rotating metallic drum collector wrapped with aluminium with a rotational speed of 300 rpm and a fixed distance of 20 cm from the needle tip. All electrospinning experiments were conducted at room temperature and constant humidity about 30% until 100 ±10 µm membrane thickness was achieved for all the samples. The as spun PAN membranes were denoted as PAN 5, PAN 8, PAN 10, and PAN 12, corresponding to the PAN concentration from 5 to 12 wt.%.

2.3. Stabilization and carbonization of PAN membranes

The electrospun PAN membranes were stabilized by oxidation in air using a fan-forced lab oven (Thermo Scientific) to chemically prepare the PAN nanofibres for the carbonization process. The membranes were thermally stabilized at fixed temperature of 250 °C, while the residence time was varied from 30 to 130 min to select the relevant time for the target extent of stabilization reaction. During the thermal stabilization process, the linear structure of PAN was converted to cyclized PAN structure. An extent of stabilization (cyclization) reaction (EOR) of 60 to 80% was commonly utilized for the preparation of high-quality carbon fibres [34, 38]. Therefore, an EOR of 70% was selected as the target EOR before the carbonization step in this work. The EOR of the stabilized membranes was calculated based on Equation 1 [34, 39], where Abs (1590) and Abs (2242) are the measured absorbances of the C=N and C≡N functional groups at wavenumbers of 1590 and 2242 cm^{-1}, respectively. The impact of residence time on the calculated EOR is presented in Fig. S1. The stabilized membranes were then carbonized inside the carbon fibre research line furnace at the Carbon Nexus in Deakin University (Fig. S2). Briefly, the stabilized membranes were fixed using tensioned carbon fibre tows, which were pulled at a line speed of 65 m/h through three-zone furnace. The furnace temperatures at the three zones were fixed at 400, 600, 800 °C, respectively under atmospheric N_2 flow to replace O_2 gas out of the furnace and avoid membrane degradation. The resulting carbonized PAN membranes were named as CNF 5, CNF 8, CNF 10, and CNF 12, corresponding to the concentration of PAN from 5 to 12 wt.%.

$$\text{Extent of cyclization reaction (EOR) (\%)} = \frac{100 \times 0.29 \times \text{Abs (1590)}}{\text{Abs (2242)} + (0.29 \times \text{Abs (1590)})} \quad (1)$$

2.4. Oxygen plasma treatment of carbon nanofibrous (CNF) membranes

The carbon nanofibrous (CNF) membranes were treated using plasma oxidation technique to improve their physicochemical properties and surface reactivity by introducing oxygen-containing functional groups on the surface of CNF membranes. The oxygen plasma treatment was conducted within Cambridge Nanotech FIJI F200 atomic layer deposition facility by allowing oxygen flow of 100 sccm at a plasma power of 300 W. The oxygen plasma exposure time was varied from 1, 3, and 5 to 7 min to investigate the impact of exposure time on the morphological, physicochemical and electrocatalytic properties of CNF membranes. The oxygen plasma treated CNF membranes were denoted as O-CNF-1, O-CNF-3, O-CNF-5, and O-CNF-7 membranes, corresponding to exposure times of 1, 3, 5, and 7 min, respectively.

2.5. Materials characterization

The morphologies of PAN, CNF, and O-CNF membranes were investigated using scanning electron Microscopy (SEM) Zeiss Supra 55VP field emission gun with an accelerating voltage of 5 KV at a working distance of 10 mm. The membranes were coated by 3 nm gold thin film using a Leica EM ACE600 sputter coater (Leica Microsystems, Australia) to minimize charging effect during the SEM imaging. The captured images were analyzed using “ImageJ” software to estimate the fibre diameter of the membranes as previously reported [40].

A capillary flow porometer (3GZH Quantachrome, Florida, U.S.A.) was utilized to determine the pore size distributions of the membranes. The mean pore size and pore size distribution were assessed by plotting the pore size versus the differential pore number percent. The membranes were cut into 25 mm diameter circular discs, followed by wet-up/dry-up setup

using Porofil as a wetting liquid. An analytical grade N_2 gas was used to apply the required pressure for liquid flow across the membranes.

The mechanical properties of CNF membranes were investigated using an Instron 30 KN tensile tester (Instron model 5967 Corporation, USA) to obtain the stress-strain curves. The tensile tester was equipped with a 50 N load cell, while the length and width of the samples were fixed at 30 and 15 mm, respectively with a tensile testing rate of 1 $mm.min^{-1}$. Three measurements were conducted for each sample, and the results were then averaged.

Thermal gravimetrical analysis (TGA) using TA Q50 instrument was utilized to assess the thermal stability of nanofibrous PAN membranes upon stabilization and carbonization processes. The membranes were heated under air at a rate of 10 °C/min from 25 to 900 °C, while the weight percent was monitored.

X-ray diffraction (XRD) patterns of CNF membranes were collected by X-ray diffractometer (XRD, PANalytical, Xpert Powder) with Cu Kα radiation of $\lambda = 0.15405$ nm and a 10 mm mask. XRD scans were conducted at 40 kV and 30 mA in the range of $2\theta = 10$ to 80° with 0.0065 step size and 300 s per step to enhance the signal to the noise ratio. The XRD patterns were then analyzed using High Score Plus software to evaluate the graphitic structure of the CNF membranes.

Fourier transform infrared (FTIR) spectrometer (Bruker Lumos) equipped with a germanium crystal, was used to monitor the chemical changes of nanofibrous PAN membranes upon stabilization, carbonization, and plasma oxidation processes. The membranes were scanned using attenuated total reflectance (ATR) mode from 600 to 4000 cm^{-1} wavenumber with 128 scans and a 4 cm^{-1} resolution.

Raman spectroscopy was used to investigate the chemical structure of as-spun, stabilized, and carbonized PAN membranes. Raman spectroscopy was conducted by Renishaw Raman spectroscopy by fixing the samples on glass substrates covered by aluminium foil. The measurements were performed using a 50x objective and 514 nm argon ion laser. The laser power was reduced to 50% to avoid sample damage. The spectra were then collected over exposure time of 20 seconds and 3 accumulations.

X-ray photoelectron spectroscopy (XPS) analysis was performed at RMIT University to evaluate the surface chemistry of CNF and O-CNF membranes. XPS analysis was carried out on a Kratos Axis Supra utilizing a monochromatized Al Kα X-ray Source (E photon = 1486.7 eV) at a pressure around 5×10^{-8} Torr. The samples were mounted on sticky carbon tape and maintained under high vacuum (2×10^{-7} Torr) for 2 h. High resolution spectra were collected at 40 eV pass energy with 0.1 eV step size, 100 ms dwell time and 20 scans. The data analysis was then conducted using CasaXPS software by applying Shirley background. Relative Sensitivity Factor (RSF) of each element was determined using the software library for quantitative analysis. Element calibration was employed with respect to the carbon peak centred at 284.6 eV [41]. The high-resolution spectrum of each element was then deconvoluted using CasaXPS software, while mixed Gaussian-Lorentzian functions (GL30) were employed to fit the deconvoluted peaks.

The streaming potential of CNF and O-CNF membranes was measured using an Electrokinetic Analyzer SurPASS 3 with a gap cell (Anton Paar, Australia) to evaluate the surface charge of the membranes. The membrane streaming potential was determined within a pH range between 2 to 11 using 0.1 M KCl electrolyte, 0.1 M HCl, and 0.1 M KOH titrants. Three measurements were recorded for each membrane at different pH values, and the average values were then calculated to analyze the membrane streaming potential.

Water contact angle of CNF and O-CNF membranes was measured using Biolin Scientific goniometer and 3 µL drop of deionized water to assess the membrane hydrophilicity. The drop images were captured after 15 s of drop impact on the membrane surface. The data analysis was conducted by OneAttension Theta Lite software. The contact angles on both sides of the drop were estimated by fitting the drop image to the Young's Laplace equations, followed by averaging the estimated values.

The electrochemical properties of CNF and O-CNF membranes were analyzed using three-electrode system connected to a potentiostat (BioLogic SP-300, France) electrochemical workstation. The synthesized membranes were used as working electrodes, while graphite rod and Ag/AgCl (in 3.5 M KCl) were used as counter and reference electrodes, respectively. Linear sweep voltammetry testing was conducted using 0.1 M Na_2SO_4 electrolyte solution to record the current density at a varied scanning voltage from 0 to 2.5 V vs Ag/AgCl with a scan rate of 20 $mV.s^{-1}$. The maximum current density and oxygen evolution potential (OEP) were then deduced from the linear sweep voltammograms as reported elsewhere [37, 42].

2.6. Electrocatalytic membrane reactor setup and performance testing

The performance of CNF and O-CNF membranes was investigated using a laboratory-scale electrocatalytic membrane reactor (ECMR) combined with cross-flow filtration system as depicted in Fig. S3. The CNF and O-CNF membranes with an effective membrane area of 25 cm^2 were used as electrocatalytic membrane anodes, connected to the positive terminal of a DC power supply (RIGOL DP832- 30V/3A, Beijing, China). A titanium (Ti) mesh with a pore size of 77 µm was connected to the negative terminal of the DC power supply to act as a cathode in the ECMR. Both electrodes were mounted inside the reactor and separated utilizing a 1 mm thick

poly(dimethylsiloxane) (PDMS) separator. Methylene blue (MB) (5 ppm) and acetaminophen (ACP) (20 ppm) aqueous solutions were used as model organic pollutants to assess the separation and electrocatalytic performance of the fabricated membranes. A peristaltic pump was connected to the feed line to circulate the organic pollutant solution from the feed container to the reactor with a 200-rpm circulation speed. A supporting electrolyte solution of 0.1 M Na_2SO_4 was provided in the feed solution to provide ionic conductivity to the analyzed solutions during the electrocatalytic reaction [43]. The membrane reactor was operated in three modes, including batch electrocatalysis (EC), cross-flow microfiltration (MF) and cross-flow microfiltration combined with electrocatalysis (MF/EC) to evaluate the membrane performance at different operating modes.

In batch-type EC mode, 10 mL of the model organic pollutant was also kept inside the membrane reactor, while a potential difference of 2 V was applied between CNF membrane anode and Ti mesh cathode using the DC power supply. In this mode, an operating pressure was not applied to avoid permeation across the membrane so that the electrocatalytic properties of CNF membranes can be evaluated without the impact membrane filtration. The electrocatalytic reaction was conducted in dark to avoid the impact of light during the electrocatalytic reaction. At fixed time interval of 30 min, 2 mL aliquot of organic pollutant solution was pipetted from the reactor to a quartz cuvette for analysis using USB-2000 UV-Visible spectrophotometer (Ocean Optics, United States) to measure the variations in the concentrations of MB and ACP solutions.

In cross-flow MF mode, the feed solution was circulated inside the reactor, while the retentate was recirculated back to the feed tank. An applied pressure of 20 kPa was then provided to allow the solution permeation across the CNF membranes. The water permeance was determined based on Equation 2 [44]:

$$\text{Water permeance} = \frac{\text{permeate volume (L)}}{(\text{membrane area } (m^2)) \times (\text{time (min)}) \times (\text{pressure (bar)})} \quad (2)$$

The permeate solutions were then analyzed using the UV-Visible spectrophotometer to measure the solute rejection percent of MB and ACP, respectively using Equation 3 [45]:

$$\text{Solute rejection \%} = \left(1 - \frac{C_p}{C_f}\right) \times 100 \quad (3)$$

Where C_p and C_f represent the concentrations of the permeate and feed solutions, respectively.

In combined microfiltration with electrocatalysis (MF/EC) mode, cross-flow MF process was operated at an applied potential difference of 2 V between the active electrodes. Consequently, simultaneous separation and electrocatalytic degradation of organic pollutants can be attained. The feed solution was circulated inside the membrane reactor, while both the retentate and permeate solutions were recirculated back to the feed tank. At fixed time interval of 30 min, 2 mL aliquot of organic pollutant solution was collected from the permeate side to a quartz cuvette for analysis using UV-Visible spectrophotometer as previously explained.

3. Results and discussion

The morphology and structural properties of CNF membranes are discussed and correlated with the concentration of PAN precursor in the dope solutions. The impact of oxygen plasma treatment on the physicochemical and electrochemical properties of O-CNF membranes is then explained and linked to their separation and electrocatalytic performance. The suggested mechanisms for the separation and electrocatalytic degradation of model organic pollutants are then provided based on the surface chemistry and electrochemical properties of the synthesized CNF and O-CNF membranes.

3.1. Morphological and structural properties of CNF membranes

The morphology of macroporous CNF membranes synthesized from different PAN concentrations (5 to 12 wt.%) is presented across the SEMs in Fig. 1a-d, while the SEM images of pristine, stabilized, and carbonized PAN with different PAN concentrations are shown in Fig. S4 for reference. At lower PAN concentration of 5 wt.%, deformed and discontinuous fibres were observed in the CNF 5 membrane network, while more stable uniform nanofibrous networks were achieved at higher PAN concentrations. Therefore, higher PAN concentrations above 5 wt.% were required to avoid fibre deformation and discontinuity upon thermal stabilization and carbonization at high temperature above 800 °C [46]. The mean pore size and fibre diameter of the CNF membranes were found to increase consistently with greater PAN concentration in the dope solutions from 5 to 12 wt.% as shown in Fig. 1e and f. The CNF fibre diameter was increased from 72.1 to 428.9 nm with PAN concentration from 5 to 12 wt.%, respectively due to the generation of more tangled polymer chains, which would result in larger CNF fibre diameters [47]. Similarly, the mean pore size of the CNF membranes increased from 0.40 to 3.16 µm with increasing the

CNF fibre diameters due to packing restrictions associated with larger fibre deposition by traditional electrospinning as reported in the literature [48-50].

The stress-strain curves of the CNF membranes with different PAN concentrations are presented in Fig. 1g to evaluate their mechanical properties. The mechanical properties of CNF membranes were significantly enhanced upon increasing the concentration of PAN from 5 to 12 wt.%. The CNF 12 membrane was found to exhibit a modulus of elasticity about 344 MPa and elongation at break around 8%, which was 4 times higher than the CNF 5 membranes with an elasticity modulus and an elongation percent of only 82 MP and 2%, respectively. Interestingly, a tensile strength of 13.7 MPa was exhibited by CNF 12 membrane that was 11 times higher than CNF 5 membrane with only 1.2 MPa. Such significant improvement in the mechanical properties upon increasing PAN concentration validates that the mechanical stability and flexibility of CNF membranes can be optimized with increasing PAN concentration in the dope solutions [34, 51, 52]. Therefore, the resulting CNF 12 membranes were selected to conduct the subsequent oxygen plasma treatment and performance testing due to their enhanced mechanical properties. Such flexible resilient CNF membranes were required to avoid any accidental damage or break of the membranes during the filtration and electrocatalytic remediation of contaminated water.

3.2. Morphology and chemical composition of O-CNF membranes

The large area macroporous CNF membranes were treated using oxygen plasma oxidation to improve their surface reactivity and wettability by introducing oxygen functional groups on the membrane surfaces [53-55]. The morphology of oxygen plasma-treated CNF membranes is presented in Fig. 2a-e. Rougher carbon nanofibres were observed with increasing the oxygen plasma exposure time from 1 min (O-CNF-1) to 7 min (O-CNF-7) due to the etching impact of ion

bombardment during oxygen plasma treatment [55]. The impact of oxygen plasma treatment on CNF chemistry was presented by FTIR analysis. As shown in FTIR spectra in Fig. 2f, the O–H (3105 cm^{-1}) and C=O (1709 cm^{-1}) stretching vibration peaks were evolved upon increasing the oxygen plasma exposure time from 1 to 7 min, corresponding to O-CNF-1 to O-CNF-7, respectively [55-57]. Thus, the production of sufficient oxygen-containing functional groups on the CNF membrane surfaces upon oxygen plasma treatment was verified.

The presence of oxygen-containing functional groups on CNF membranes was further assessed using XPS analysis to identify the surface chemistry and chemical composition of O-CNF membranes (Fig. 3, S9, and Table S1). In Fig. 3a-c, the C 1s spectrum of CNF membranes was deconvoluted into 6 peaks, including graphitic carbon C=C (284.4 eV), amorphous carbon C–C (285.3 eV), C–O/C–N (286.3 eV), C=O (287.8 eV), O–C=O (289.1 eV), and π–π^* transition (292.0 eV) [58, 59]. The contribution of oxidized carbon moieties was boosted with increasing the plasma exposure time from 0 to 5 min, while the intensity of amorphous carbon C–C peak was increased on the expense of graphitic carbon C=C peak. Thus, an effective reaction of oxygen plasma with the carbon nanofibres was validated. As presented in the N 1s spectrum of CNF membranes in Fig. 3d-f, 4 deconvoluted peaks were attributed to pyridinic N (398.2 eV), pyrrolic N (399.9 eV), graphitic N (401.1 eV), and oxidized N (402.5 eV) [58, 60, 61]. The intensity of oxidized N peak was also raised with oxygen plasma treatment due to the reaction with oxygen-containing groups generated on CNF membranes. In Fig. 3g-i, the O 1s spectrum of CNF membranes was fitted into 4 peaks, including O–C/O–H (532.1 eV), C=O (531.0 eV), O–C=O (533.2 eV), and H_2O (535.3 eV) [59, 62]. The intensities of O–C/O–H, and H_2O peaks were increased with oxygen plasma exposure from 0 to 5 min in agreement with the FTIR analysis. The above XPS analysis confirms the successful functionalization of CNF membranes with oxygen-containing groups after oxygen

plasma treatment, while O–C and O–H moieties are predominately attached to the carbon nanofibres. The attachment of oxygen-containing functional groups on CNF membrane surface may induce the physicochemical and electrochemical properties of CNF membranes [63-65].

3.3. Physicochemical and electrochemical properties of O-CNF membranes

The physicochemical properties of CNF and O-CNF membranes were investigated to evaluate their surface charge and wettability, which govern the interactions between the membranes and organic pollutants present in aqueous solutions. The streaming potential of CNF and O-CNF membranes was assessed to determine their surface charges across a pH range from 2 to 11 (Fig. 4a). The streaming zeta potential of pristine CNF membrane was increased negatively by 55% to reach -31 mV at pH 6 after 1 min of oxygen plasma exposure. Extended plasma exposure time was found to induce the formation of more negative charges on the O-CNF membrane surface charge, leading to more negative streaming potentials of -40 and -45 mV at pH 6 for O-CNF-5 and O-CNF-7, respectively. The isoelectric point of pristine CNF membranes was also shifted from a pH of 4.6 to 2.8 and 2.5 upon increasing the plasma exposure time to 5 and 7 min, respectively. Thus, more negative charges were generated on the O-CNF membranes across wider pH range. This negative shift can be explained by the production of oxygen-containing functional groups on CNF surfaces upon oxygen plasma treatment as explained in the FTIR and XPS analysis [66-68]. The presence of negative surface charges on the CNF membrane surface may improve the electrostatic interactions with the cationic organic contaminants in wastewater [69, 70]. The membrane surface wettability can be also enhanced with presence of negative charges on CNF surface [71]. Thus, water contact angle measurements were conducted to investigate the changes in the CNF surface wettability upon oxygen plasma treatment, which is an essential

property required in water purification applications [71, 72]. The water contact angle of pristine CNF membranes (135.7°) was significantly reduced with increasing the oxygen plasma exposure time from 1 to 7 min to stabilize around 24° for O-CNF-5 and O-CNF-7 membranes, and this was associated with a consistent increase in the oxygen content on CNF surface up to 20 at.% (Fig. 4b). Hence, the reduced water contact angle was attributed to the improved surface hydrophilicity with the introduction of oxygen-containing functional groups upon oxygen plasma treatment [73, 74].

The electrochemical properties of O-CNF membranes were investigated using linear sweep voltammetry (LSV) technique to determine the variation in the maximum current density and oxygen evolution potential (OEP) with oxygen plasma treatment. Fig. 4c and S10 present the LSV polarization plots of pristine CNF and O-CNF membranes with a varied plasma exposure time from 1 to 7 min. The maximum current density was raised with oxygen plasma to reach up to ~20 $mA.cm^{-2}$ after plasma exposure of 5 to 7 min, which was 2 times higher than that of the pristine CNF membrane (Fig. 4d). The raised current density was attributed to the reduced charge transfer resistance with the presence of oxygen-containing functional groups on O-CNF membranes [75, 76]. In addition, the OEP of pristine CNF membranes was shifted from 1.29 V to higher OEP up to 1.62 V with plasma exposure of 5 to 7 min, which agreed with relevant reported studies in the literature [29, 37]. The higher OEP may improve the electrocatalytic performance of O-CNF towards pollutant degradation rather than the competitive oxygen evolution reaction, and hence, the current efficiency can be improved at lower energy consumption [77-79].

3.4. Separation and electrocatalytic performance of O-CNF membranes (cross-flow MF/EC)

The macroporous O-CNF membranes were investigated in cross-flow filtration MF/EC mode to evaluate their potential for pollutants removal from synthetic water effluents. The O-CNF membranes were first investigated in crossflow MF mode without applying an electric field to assess their performance for the removal of MB and ACP pollutants via microfiltration alone. The pure water flux across the O-CNF membranes was determined at an applied pressure of 20 kPa to evaluate the water permeance performance across the membranes. The impact of oxygen content on the water permeance of O-CNF membranes is demonstrated in Fig. 5a. The water permeance of O-CNF membranes was gradually enhanced with increasing the oxygen content to reach 4.65 $\times 10^3$ $L.m^{-2}.h^{-1}.bar^{-1}$ with ~20 at.% oxygen after 5 min of plasma exposure, which was higher by 40% than that of pristine CNF membranes. The water permeance was then plateaued at 4.82 $\times 10^3$ $L.m^{-2}.h^{-1}.bar^{-1}$ with further increase in the plasma exposure time to 7 min, indicating the saturation of CNF surface with oxygen-containing groups with plasma exposure beyond 5 min. Such high water permeance of O-CNF membranes was also 4.5 to 21.5 times higher than relevant electrospun ZnO/ PAN and SnO_2/CNF membranes, respectively in the literature [13, 30]. The enhanced water permeance with oxygen plasma treatment can be attributed to the improved surface wettability with the introduction of oxygen-containing groups on CNF membrane surface [80-82]. The solute rejection performance of O-CNF membranes was also investigated to analyze their selectivity and sieving properties against MB and ACP pollutants (Fig. 5b). The pristine CNF membranes were found to remove only 29.2% and 3.8% of MB and ACP, respectively during the microfiltration process since their pore size (~ 3.2 µm) was much larger than MB and ACP sizes [83-85]. Thus, the achieved small solute rejection percent can be explained by π-π interactions between the carbon nanofibres and the organic pollutants [86-88]. Interestingly, oxygen plasma treatment was found

to improve the rejection of MB and ACP by 1.4 to 2.4 times to reach 41% and 9%, respectively with increasing the oxygen content to ~20 at.%. The improved MB rejection was attributed to electrostatic interactions between the generated negative charges on O-CNF membranes and the cationic MB dyes [89, 90], while the enhanced ACP rejection was explained by the hydrophilic interactions with the oxygen-containing groups on O-CNF membrane surface [91, 92].

The performance of O-CNF membranes was then investigated for simultaneous microfiltration and electrocatalytic degradation of MB and ACP under cross-flow MF/EC mode and benchmarked with batch electrocatalytic (EC) mode (Fig. S11, S12, and Table S2). A potential difference of 2 V was applied between O-CNF membrane anodes and Ti mesh cathodes for the degradation of 5 ppm MB and 20 ppm ACP, respectively. The MF/EC reaction kinetics for MB and ACP degradation were found to follow pseudo first order reaction kinetics (Fig. S12). As presented in Fig. 5c, the MF/EC reaction kinetic constants for MB and ACP removal were gradually increased with increasing the oxygen content to ~20 at.% with plasma exposure time up to 5 min to reach 29.6×10^{-3} and 15.6×10^{-3} min^{-1}, respectively. The MF/EC reaction kinetic constants for MB and ACP removal were 2.4 and 1.7 times higher than the reaction kinetic constants exhibited by EC alone, respectively. However, the MF/EC reaction kinetic constant was then plateaued with increasing the plasma exposure time above 5 min due to the saturation of CNF membrane surface with oxygen-containing groups [93, 94]. The enhancement in the reaction kinetic constant upon oxygen plasma treatment can be explained by the elevated OEP and current efficiency arising from the generated catalytic active sites of oxygen-containing functional groups on the CNF surface [36, 95, 96]. It was also found that 99% of MB and 91% of ACP were removed during MF/EC process after 2.5 h, and thus outperforming other relevant CNF materials in the literature as explained in Table 1. Such high removal efficiency under MF/EC mode was 2.4 to

10.3 times higher than the removal efficiency attained under MF alone against MB and ACP, respectively (Table S3). The stability and reusability of the synthesized O-CNF-5 membranes during MF/EC removal of MB and ACP were also evaluated to validate the process scalability in practical water treatment. The MF/EC reaction kinetics were investigated over 8 reuse cycles for the removal of MB and ACP, respectively (Fig. S13). The reaction kinetic constants for MB and ACP degradation were quite stable even after 8 runs under cross-flow MF/EC mode (Fig. 5d). The MF/EC reaction kinetic constants for MB and ACP removal were reduced by only 4.4×10^{-3} and 2.4×10^{-3} min^{-1}, respectively. In addition, the XPS analysis after MF/EC reaction revealed the high stability of O-CNF membranes without any significant chemical changes, while the contribution of oxidized carbon moieties was increased due to the adsorption of generated hydroxyl radicals during MF/EC process (Fig. S14 and S15) [97, 98]. Such high-performance stability emphasizes the potential of O-CNF membranes in the development of durable O-CNF MF membranes with self-cleaning capability.

The considerable improvement in the reaction kinetics and their stability during MF/EC mode validate the potential of oxygen plasma treated CNF membranes towards simultaneous microfiltration and electrocatalytic degradation of organic pollutants as illustrated in Fig. 6. The application of a potential difference between Ti cathode and O-CNF membrane anode induces the production of electron-hole pairs on the active anode. The positive holes can act as strong oxidizing agents for the adsorbed organic pollutants and water molecules on the surface of O-CNF membranes [99, 100]. The improved wettability of O-CNF membranes via oxygen plasma treatment promotes a strong interaction between the electrolyte solution and the active catalytic sites on O-CNF membrane anodes [101, 102]. The generation of oxygen-containing groups on O-CNF membranes also enhances the ionic interactions with MB pollutant via π-π interaction and

electrostatic attraction [84, 86, 90], while the interaction with ACP pollutant was promoted via hydrogen bonding [87, 102]. The captured organic pollutants on O-CNF surface can be then oxidized via direct or indirect oxidation pathways into H_2O and CO_2, while the competitive oxygen evolution reaction can be retarded by raising the OEP of O-CNF membranes via oxygen plasma treatment [21, 35, 36]. During the direct oxidation, O-CNF can be excited by applying a potential difference between the active electrodes, leading to the generation of electron-hole pairs [22, 29]. The positive holes can act as strong oxidizing agents to the adsorbed organic pollutant molecules, degrading them into H_2O and CO_2 [103, 104]. On the contrary, indirect oxidation is another possible pathway for the degradation of organic pollutants on O-CNF anode surface by the adsorption and oxidation of H_2O molecules on the O-CNF anode surface to active $^{\bullet}OH$ radicals [105, 106]. The active $^{\bullet}OH$ radicals can be then utilized to oxidize the adsorbed organic contaminants on the O-CNF anode surface, while the CNF can act as a conductor to transfer the generated electrons and accelerate the electrocatalytic degradation reaction rate [107-109]. Furthermore, the presence of oxygen-containing functional groups and improved wettability of O-CNF membrane anodes upon oxygen plasma treatment would facilitate the adsorption of the reactive hydroxyl radicals for efficient degradation of organic pollutants [102].

4. Conclusions and prospects

In this work, an innovative stepwise methodology was developed to synthesize flexible microfiltration carbon nanofibre membranes with fine-tuned wettability and surface reactivity via oxygen plasma treatment for effective separation and electrocatalytic degradation of emerging organic pollutants. The CNF membrane wettability and surface reactivity were enhanced by introducing oxygen-containing functional groups on CNF membrane surface via oxygen plasma treatment. The water contact angle of O-CNF membranes was reduced to 24° after plasma exposure for 5 min, leading to a high water permeance of 4.65×10^3 $L.m^{-2}.h^{-1}.bar^{-1}$ across the membranes. The introduction of oxygen plasma was also found to enhance the electrocatalytic properties of O-CNF membranes by raising their electro-oxidation capacity and oxygen evolution potential up to 1.62 V with increasing the oxygen content on CNF surface to ~20 at.%.

The improved surface reactivity and electrocatalytic properties of O-CNF membranes were found to synergistically boost the removal efficiency against MB and ACP up to 99 and 91% under MF/EC mode with reaction kinetic constants 29.6×10^{-3} and 15.6×10^{-3} min^{-1}, respectively. Such high reaction kinetic constants were kept stable even after 8 reuse cycles to demonstrate the capability of O-CNF membranes for cost-effective water purification, outperforming other relevant CNF membranes in the literature. The current study offers a scaled-up fabrication scheme of functional microfiltration CNF membranes with enhanced mechanical flexibility and electrocatalytic performance to support the intensification of electrocatalytic membrane reactors.

Acknowledgement

This work was conducted in part at the Melbourne Centre for Nanofabrication (MCN) in the Victorian Node of the Australian National Fabrication Facility (ANFF). The Advanced Characterisation Facility at Deakin University is acknowledged for utilizing the Electron Microscopy instruments. The authors acknowledge the Carbon Nexus operation team for their help during the fabrication of CNF membranes. The authors acknowledge the scientific and technical assistance of the RMIT University's Microscopy and Microanalysis Facility, a linked laboratory of the Microscopy Australia. The authors also acknowledge LINTEC OF AMERICA, INC for funding this research work. AM acknowledges the Australian Research Council for financial support (DP200100313). Partial financial support from Khalifa University through project RC2-2019-007 is gratefully acknowledged by LFD.

Figures and Tables

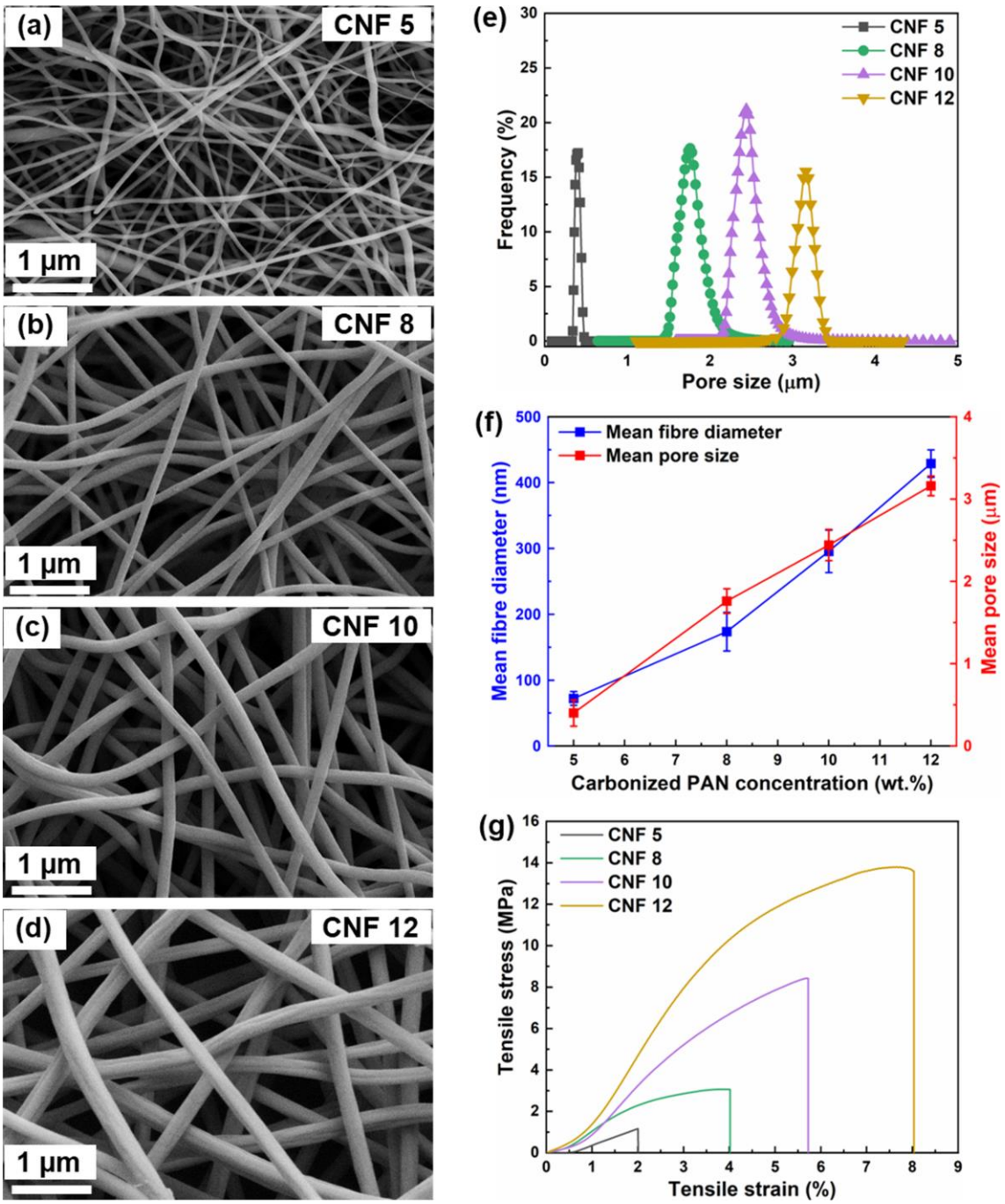

Fig. 1. SEM images of (a) CNF 5, (b) CNF 8, (c) CNF 10 and (d) CNF 12. (e) The pore size distribution of CNF membranes with different PAN concentrations from 5 to 12 wt.%. (f) The variation in mean fibre diameter and pore size of CNF membranes with different varied PAN concentrations from 5 to 12 wt.%. (f) Stress-strain curves of CNF 5, CNF 8, CNF 10, and CNF 12.

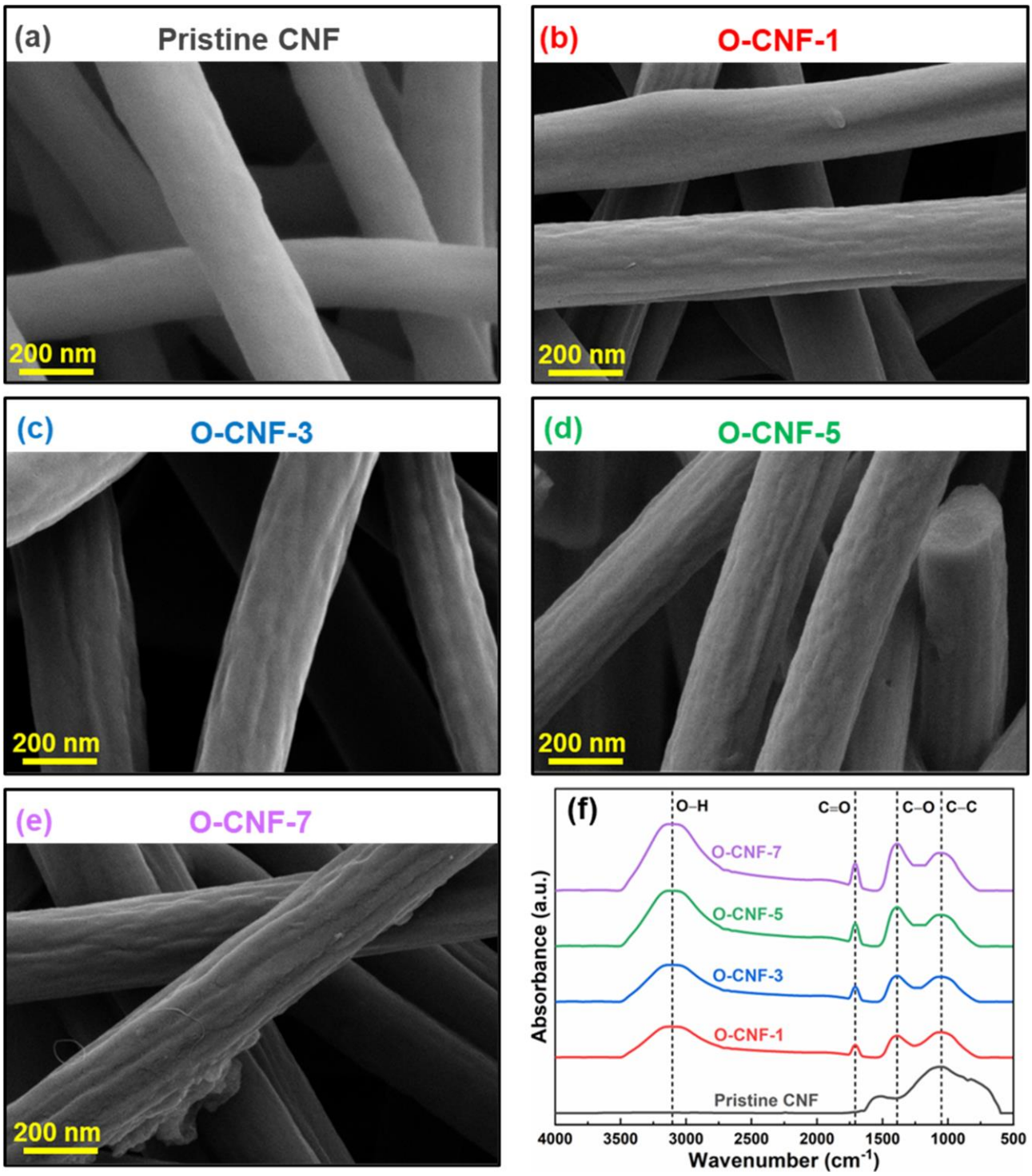

Fig. 2. (a-e) The SEM morphology of pristine CNF and O-CNF membranes with a varied plasma exposure time from 1 to 7 min. (f) FTIR spectra of pristine CNF and O-CNF membranes with different plasma exposure times from 1 to 7 min.

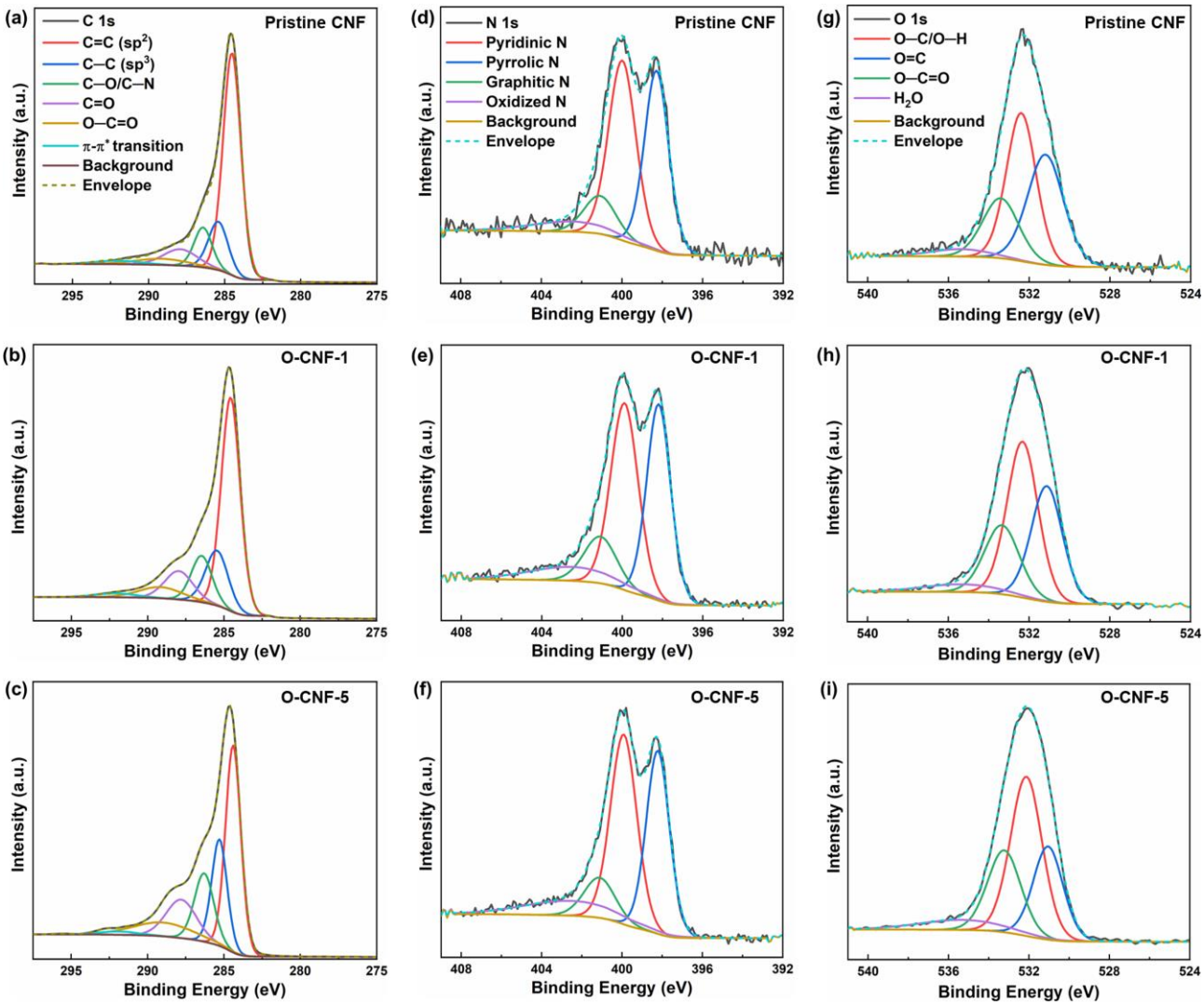

Fig. 3. (a-c) The high resolution deconvoluted peaks of XPS C 1s spectra for pristine CNF and O-CNF membranes. (d-f) The high resolution deconvoluted peaks of XPS N 1s spectra for pristine CNF and O-CNF membranes. (g-i) The high resolution deconvoluted peaks of XPS O 1s spectra for pristine CNF and O-CNF membranes.

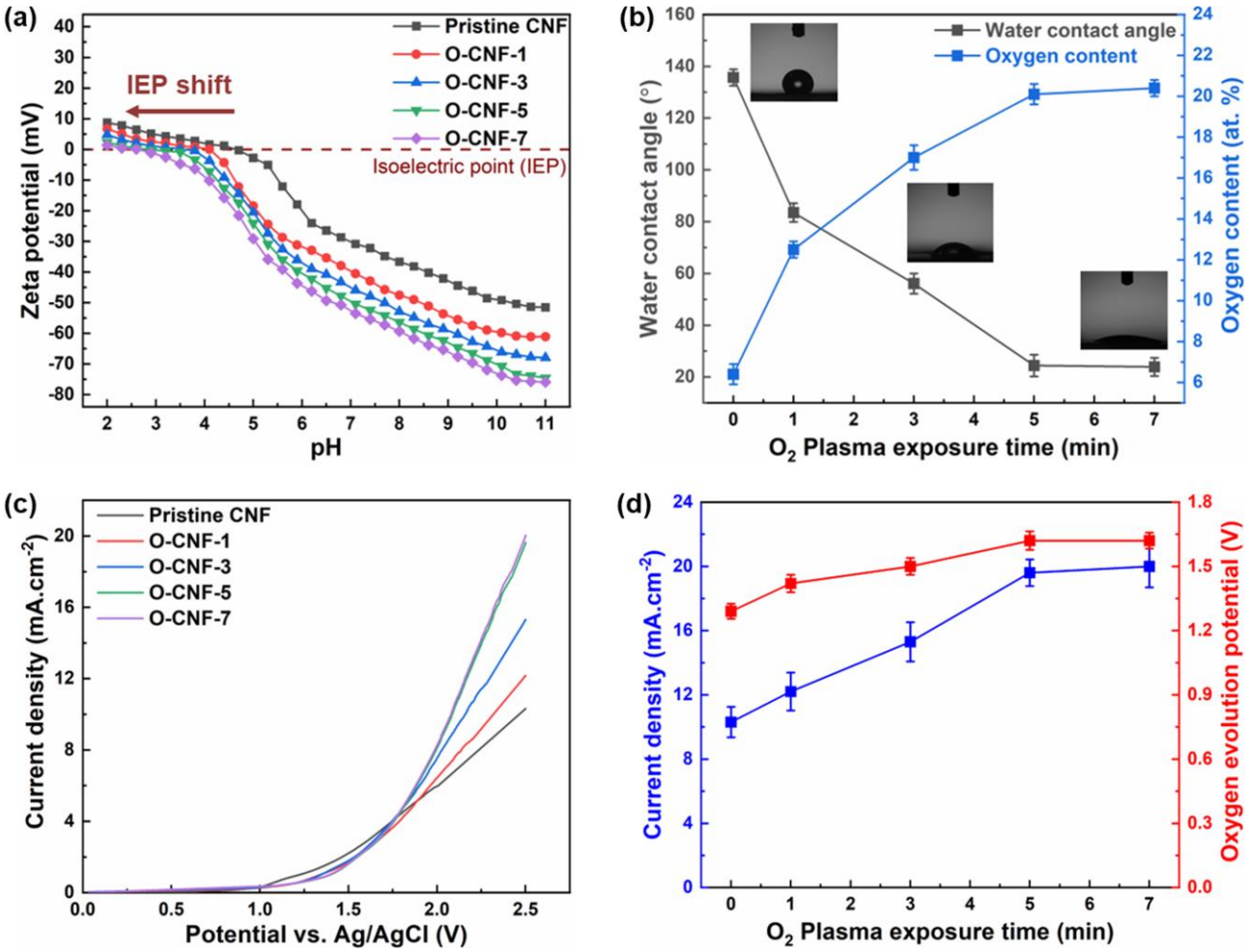

Fig. 4. (a) The variation of zeta potential of CNF and O-CNF membranes with different pH values. (b) The change in water contact angle and oxygen content of O-CNF membranes with oxygen plasma exposure time. (c) Linear sweep voltammograms of CNF and O-CNF membranes with different plasma exposure times from 1 to 7 min. (d) The variation of current density and oxygen evolution potential with oxygen plasma exposure time from 1 to 7 min.

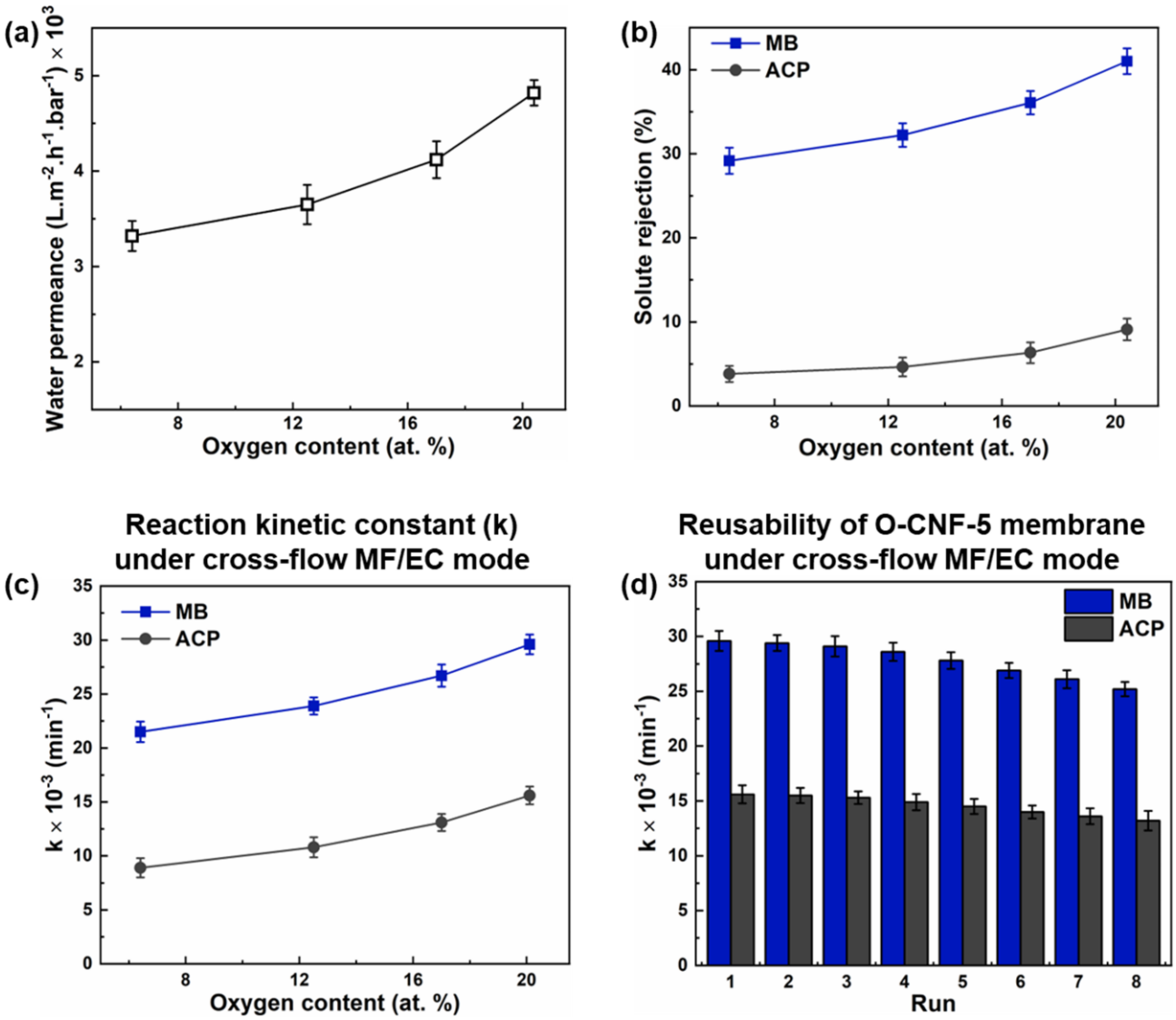

Fig. 5. (a) The variation of water permeance of CNF membranes with oxygen content. (b) The change in solute rejection of CNF membranes with oxygen content for the rejection of MB and ACP, respectively. (c) The change in the reaction kinetic constant with oxygen content under cross-flow MF/EC mode. (d) The decrease in the reaction kinetic constant for MB and ACP removal over 8 continuous cycles using O-CNF-5 membranes under cross-flow MF/EC mode.

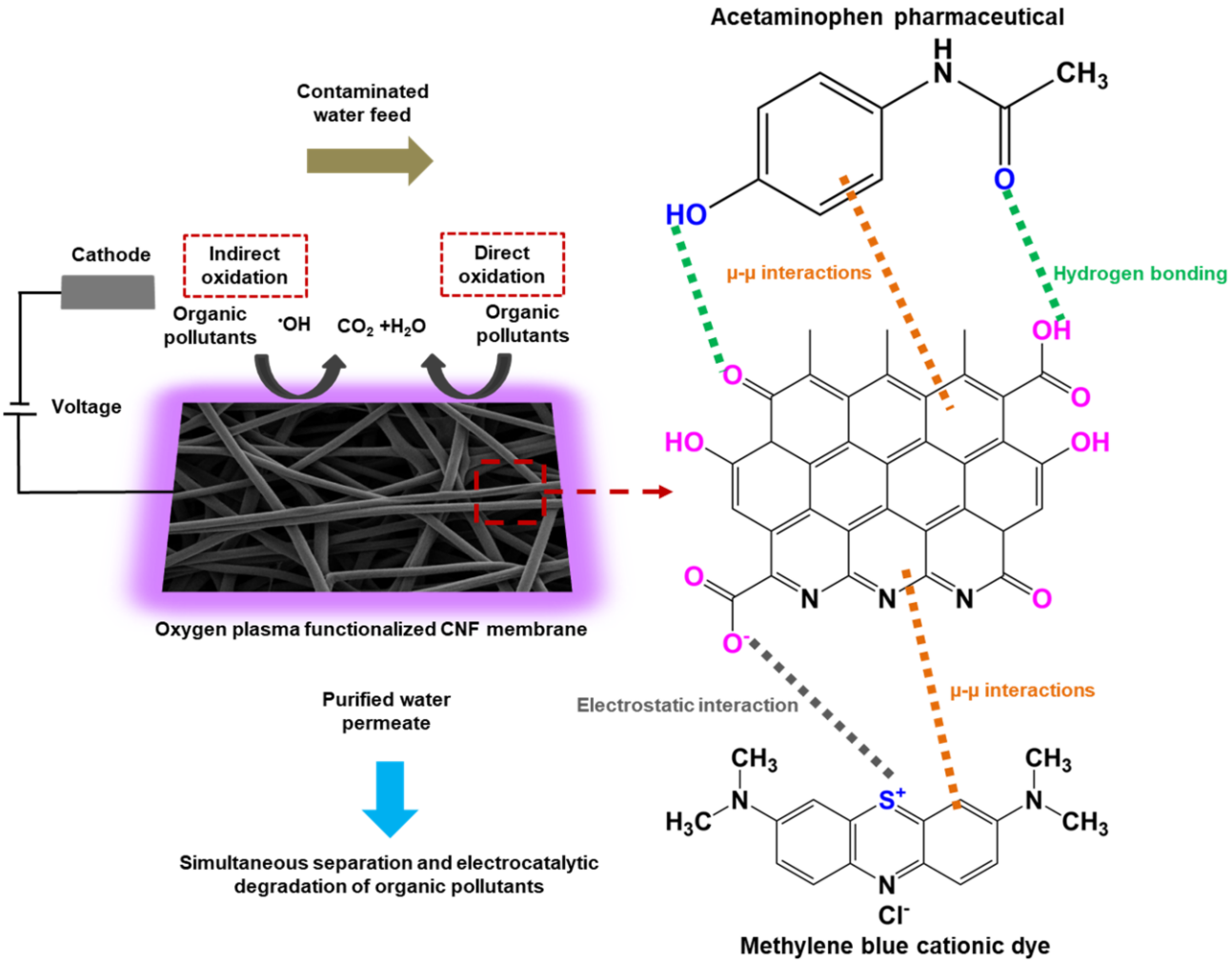

Fig. 6. The postulated mechanism for separation and electrocatalytic degradation of organic pollutants using oxygen plasma treated CNF membrane anodes at an applied cell voltage between the active CNF membrane anode and Ti mesh cathode.

Table 1. A comparison between the synthesized O-CNF membrane anodes in this work with relevant PAN-based and carbon nanofibre-based membrane anodes in the literature for the removal of different organic pollutants, including dyes and pharmaceuticals.

Membrane anode	**Organic pollutant**	**Applied voltage or current**	**Electrolyte**	**Water permeance ($L.m^{-2}.h^{-1}.bar^{-1}$)**	**Reaction kinetic constant (k) (10^{-3} min^{-1})**	**Reference**
ZnO/PAN nanofibres	20 ppm Methylene blue	15 V	0.17 M NaCl	1016	4.9	[13]
CNT/CNF	10 ppm Methylene blue	50 mA	0.1 M H_2SO_4	–	7.6	[110]
CNF	200 ppm Acetaminophen	3.5 V	0.1 M Na_2SO_4	–	5.1	[29]
O_2-CNF	200 ppm Acetaminophen	3.5 V	0.1 M Na_2SO_4	–	25.7	[29]
Fe-Co/CNF	30 ppm Tetracycline	1 V	0.1 M Na_2SO_4	–	9.5	[35]
SnO_2/CNF	10 ppm Sulfamethoxazole	1 V	0.01 M NaCl	216.4	3.9	[30]
O-CNF-5	5 ppm Methylene blue	2 V	0.1 M Na_2SO_4	4650	29.6	This work
O-CNF-5	20 ppm Acetaminophen	2 V	0.1 M Na_2SO_4	4650	15.6	This work

References

[1] K. Aruchamy, K. Dharmalingam, C.W. Lee, D. Mondal, N. Sanna Kotrappanavar, Creating ultrahigh surface area functional carbon from biomass for high performance supercapacitor and facile removal of emerging pollutants, Chemical Engineering Journal 427 (2022). https://doi.org/10.1016/j.cej.2021.131477.

[2] Y. Wang, I. Zucker, C. Boo, M. Elimelech, Removal of Emerging Wastewater Organic Contaminants by Polyelectrolyte Multilayer Nanofiltration Membranes with Tailored Selectivity, ACS ES&T Engineering 1(3) (2021) 404-414. https://doi.org/10.1021/acsestengg.0c00160.

[3] J. Aravind kumar, T. Krithiga, S. Sathish, A.A. Renita, D. Prabu, S. Lokesh, R. Geetha, S.K.R. Namasivayam, M. Sillanpaa, Persistent organic pollutants in water resources: Fate, occurrence, characterization and risk analysis, Science of The Total Environment 831 (2022) 154808. https://doi.org/10.1016/j.scitotenv.2022.154808.

[4] J. Cai, B. Niu, Q. Xie, N. Lu, S. Huang, G. Zhao, J. Zhao, Accurate Removal of Toxic Organic Pollutants from Complex Water Matrices, Environmental Science & Technology 56(5) (2022) 2917-2935. https://doi.org/10.1021/acs.est.1c07824.

[5] I. Ali, V.K. Gupta, Advances in water treatment by adsorption technology, Nature Protocols 1(6) (2006) 2661-2667. https://doi.org/10.1038/nprot.2006.370.

[6] M. Li, A. Zamyadi, W. Zhang, L.F. Dumée, L. Gao, Algae-based water treatment: A promising and sustainable approach, Journal of Water Process Engineering 46 (2022) 102630. https://doi.org/10.1016/j.jwpe.2022.102630.

[7] V.I. Parvulescu, F. Epron, H. Garcia, P. Granger, Recent Progress and Prospects in Catalytic Water Treatment, Chemical Reviews 122(3) (2022) 2981-3121. https://doi.org/10.1021/acs.chemrev.1c00527.

[8] J.R. Werber, C.O. Osuji, M. Elimelech, Materials for next-generation desalination and water purification membranes, Nature Reviews Materials 1(5) (2016) 16018. https://doi.org/10.1038/natrevmats.2016.18.

[9] S.F. Anis, R. Hashaikeh, N. Hilal, Microfiltration membrane processes: A review of research trends over the past decade, Journal of Water Process Engineering 32 (2019) 100941. https://doi.org/10.1016/j.jwpe.2019.100941.

[10] P.H. Presumido, L.F.d. Santos, T. Neuparth, M.M. Santos, M. Feliciano, A. Primo, H. Garcia, M. B- Đolić, V.J.P. Vilar, A Novel ceramic tubular membrane coated with a continuous graphene-TiO2 nanocomposite thin-film for CECs mitigation, Chemical Engineering Journal 430 (2022) 132639. https://doi.org/10.1016/j.cej.2021.132639.

[11] Y. Ren, Y. Ma, G. Min, W. Zhang, L. Lv, W. Zhang, A mini review of multifunctional ultrafiltration membranes for wastewater decontamination: Additional functions of adsorption and catalytic oxidation, Science of The Total Environment 762 (2021) 143083. https://doi.org/10.1016/j.scitotenv.2020.143083.

[12] S. Al Aani, T.N. Mustafa, N. Hilal, Ultrafiltration membranes for wastewater and water process engineering: A comprehensive statistical review over the past decade, Journal of Water Process Engineering 35 (2020) 101241. https://doi.org/10.1016/j.jwpe.2020.101241.

[13] N. Li, W. Wang, L. Zhu, W. Cui, X. Chen, B. Zhang, Z. Zhang, A novel electro-cleanable PAN-ZnO nanofiber membrane with superior water flux and electrocatalytic properties for organic pollutant degradation, Chemical Engineering Journal 421 (2021). https://doi.org/10.1016/j.cej.2020.127857.

[14] W. Zhang, L. Ding, J. Luo, M.Y. Jaffrin, B. Tang, Membrane fouling in photocatalytic membrane reactors (PMRs) for water and wastewater treatment: A critical review, Chemical Engineering Journal 302 (2016) 446-458. https://doi.org/10.1016/j.cej.2016.05.071.
[15] D.T. Myat, M.B. Stewart, M. Mergen, O. Zhao, J.D. Orbell, S. Gray, Experimental and computational investigations of the interactions between model organic compounds and subsequent membrane fouling, Water Research 48 (2014) 108-118. https://doi.org/10.1016/j.watres.2013.09.020.
[16] T.X. Huong Le, L.F. Dumée, S. Lacour, M. Rivallin, Z. Yi, L. Kong, M. Bechelany, M. Cretin, Hybrid graphene-decorated metal hollow fibre membrane reactors for efficient electro-Fenton - Filtration co-processes, Journal of Membrane Science 587 (2019). https://doi.org/10.1016/j.memsci.2019.117182.
[17] M. Sun, X. Wang, L.R. Winter, Y. Zhao, W. Ma, T. Hedtke, J.-H. Kim, M. Elimelech, Electrified Membranes for Water Treatment Applications, ACS ES&T Engineering 1(4) (2021) 725-752. https://doi.org/10.1021/acsestengg.1c00015.
[18] P. Kumari, N. Bahadur, X.A. Conlan, M. Laleh, L. Kong, L.A. O'Dell, L.F. Dumee, A. Merenda, Atomically-thin Schottky-like photo-electrocatalytic cross-flow membrane reactors for ultrafast remediation of persistent organic pollutants, Water Res 218 (2022) 118519. https://doi.org/10.1016/j.watres.2022.118519.
[19] J. Chen, S. Fan, Y. Chen, Y. Wang, K. Bai, Z. Mai, Z. Xiao, Electrocatalytic composite membrane with deep-permeation nano structure fabricated by flowing synthesis for enhanced catalysis, Journal of Membrane Science 636 (2021) 119616. https://doi.org/10.1016/j.memsci.2021.119616.
[20] P. Kumari, N. Bahadur, M. Cretin, L. Kong, L.A. O'Dell, A. Merenda, L.F. Dumée, Electro-catalytic membrane reactors for the degradation of organic pollutants – a review, Reaction Chemistry & Engineering 6(9) (2021) 1508-1526. https://doi.org/10.1039/D1RE00091H.
[21] L. Ren, J. Ma, M. Chen, Y. Qiao, R. Dai, X. Li, Z. Wang, Recent advances in electrocatalytic membrane for the removal of micropollutants from water and wastewater, iScience 25(5) (2022) 104342. https://doi.org/10.1016/j.isci.2022.104342.
[22] Y. Jiang, H. Zhao, J. Liang, L. Yue, T. Li, Y. Luo, Q. Liu, S. Lu, A.M. Asiri, Z. Gong, X. Sun, Anodic oxidation for the degradation of organic pollutants: Anode materials, operating conditions and mechanisms. A mini review, Electrochemistry Communications 123 (2021). https://doi.org/10.1016/j.elecom.2020.106912.
[23] C. Trellu, C. Coetsier, J.C. Rouch, R. Esmilaire, M. Rivallin, M. Cretin, C. Causserand, Mineralization of organic pollutants by anodic oxidation using reactive electrochemical membrane synthesized from carbothermal reduction of TiO2, Water Res 131 (2018) 310-319. https://doi.org/10.1016/j.watres.2017.12.070.
[24] J. Lee, H. Jung, Y.S. Park, S. Woo, N. Kwon, Y. Xing, S.H. Oh, S.M. Choi, J.W. Han, B. Lim, Corrosion-engineered bimetallic oxide electrode as anode for high-efficiency anion exchange membrane water electrolyzer, Chemical Engineering Journal 420 (2021) 127670. https://doi.org/10.1016/j.cej.2020.127670.
[25] C. Zhou, Y. Wang, J. Chen, J. Niu, Porous Ti/SnO2-Sb anode as reactive electrochemical membrane for removing trace antiretroviral drug stavudine from wastewater, Environment International 133 (2019) 105157. https://doi.org/10.1016/j.envint.2019.105157.
[26] Y. Zhang, K. Wei, W. Han, X. Sun, J. Li, J. Shen, L. Wang, Improved electrochemical oxidation of tricyclazole from aqueous solution by enhancing mass transfer in a tubular porous

electrode electrocatalytic reactor, Electrochimica Acta 189 (2016) 1-8. https://doi.org/doi.org/10.1016/j.electacta.2015.10.119.
[27] S. Nayak, B.P. Chaplin, Fabrication and characterization of porous, conductive, monolithic Ti4O7 electrodes, Electrochimica Acta 263 (2018) 299-310. https://doi.org/doi.org/10.1016/j.electacta.2018.01.034.
[28] Y. Liu, Y. Ren, S. You, Electrified carbon nanotube membrane technology for water treatment, Electrochemical Membrane Technology for Water and Wastewater Treatment2022, pp. 111-140. https://doi.org/10.1016/b978-0-12-824470-8.00013-9.
[29] P. Jakobczyk, G. Skowierzak, I. Kaczmarzyk, M. Nadolska, A. Wcislo, K. Lota, R. Bogdanowicz, T. Ossowski, P. Rostkowski, G. Lota, J. Ryl, Electrocatalytic performance of oxygen-activated carbon fibre felt anodes mediating degradation mechanism of acetaminophen in aqueous environments, Chemosphere 304 (2022) 135381. https://doi.org/10.1016/j.chemosphere.2022.135381.
[30] S. Yu, Y. Gao, R. Khan, P. Liang, X. Zhang, X. Huang, Electrospun PAN-based graphene/SnO2 carbon nanofibers as anodic electrocatalysis microfiltration membrane for sulfamethoxazole degradation, Journal of Membrane Science 614 (2020). https://doi.org/10.1016/j.memsci.2020.118368.
[31] Y. Huang, Q. Deng, X. Wu, S. Wang, N, O Co-doped carbon felt for high-performance all-vanadium redox flow battery, International Journal of Hydrogen Energy 42(10) (2017) 7177-7185. https://doi.org/10.1016/j.ijhydene.2016.04.004.
[32] J. Xue, J. Xie, W. Liu, Y. Xia, Electrospun Nanofibers: New Concepts, Materials, and Applications, Acc Chem Res 50(8) (2017) 1976-1987. https://doi.org/10.1021/acs.accounts.7b00218.
[33] Y. Yang, F. Simeon, T.A. Hatton, G.C. Rutledge, Polyacrylonitrile-based electrospun carbon paper for electrode applications, Journal of Applied Polymer Science 124(5) (2012) 3861-3870. https://doi.org/10.1002/app.35485.
[34] R. Al-Attabi, Y. Morsi, J.A. Schutz, D. Cornu, M. Maghe, L.F. Dumee, Flexible and reusable carbon nano-fibre membranes for airborne contaminants capture, Sci Total Environ 754 (2021) 142231. https://doi.org/10.1016/j.scitotenv.2020.142231.
[35] W. Xie, Y. Shi, Y. Wang, Y. Zheng, H. Liu, Q. Hu, S. Wei, H. Gu, Z. Guo, Electrospun iron/cobalt alloy nanoparticles on carbon nanofibers towards exhaustive electrocatalytic degradation of tetracycline in wastewater, Chemical Engineering Journal 405 (2021). https://doi.org/10.1016/j.cej.2020.126585.
[36] X. Sun, J. Bao, K. Li, M.D. Argyle, G. Tan, H. Adidharma, K. Zhang, M. Fan, P. Ning, Advance in Using Plasma Technology for Modification or Fabrication of Carbon-Based Materials and Their Applications in Environmental, Material, and Energy Fields, Advanced Functional Materials 31(7) (2020). https://doi.org/10.1002/adfm.202006287.
[37] Y.C. Lin, C.H. Chuang, L.Y. Hsiao, M.H. Yeh, K.C. Ho, Oxygen Plasma Activation of Carbon Nanotubes-Interconnected Prussian Blue Analogue for Oxygen Evolution Reaction, ACS Appl Mater Interfaces 12(38) (2020) 42634-42643. https://doi.org/10.1021/acsami.0c07821.
[38] S. Nunna, M. Maghe, R. Rana, R.J. Varley, D.B. Knorr, Jr., J.M. Sands, C. Creighton, L.C. Henderson, M. Naebe, Time Dependent Structure and Property Evolution in Fibres during Continuous Carbon Fibre Manufacturing, Materials (Basel) 12(7) (2019). https://doi.org/10.3390/ma12071069.
[39] E. Jiang, M. Maghe, N. Zohdi, N. Amiralian, M. Naebe, B. Laycock, B.L. Fox, D.J. Martin, P.K. Annamalai, Influence of Different Nanocellulose Additives on Processing and Performance

of PAN-Based Carbon Fibers, ACS Omega 4(6) (2019) 9720-9730. https://doi.org/10.1021/acsomega.9b00266.
[40] R. Al-Attabi, J. Rodriguez-Andres, J.A. Schütz, M. Bechelany, E. des Ligneris, X. Chen, L. Kong, Y.S. Morsi, L.F. Dumée, Catalytic electrospun nano-composite membranes for virus capture and remediation, Separation and Purification Technology 229 (2019). https://doi.org/10.1016/j.seppur.2019.115806.
[41] S. Zhu, J. Liu, J. Sun, Growth of ultrathin SnO2 on carbon nanotubes by atomic layer deposition and their application in lithium ion battery anodes, Applied Surface Science 484 (2019) 600-609. https://doi.org/10.1016/j.apsusc.2019.04.163.
[42] C. Zhang, J. Lu, C. Liu, Y. Zou, L. Yuan, J. Wang, C. Yu, ZnO nanoparticles embedded in hollow carbon fiber membrane for electrochemical H2O2 production by two-electron water oxidation reaction, Environ Res 206 (2022) 112290. https://doi.org/10.1016/j.envres.2021.112290.
[43] Y. Yao, C. Zhao, M. Zhao, X. Wang, Electrocatalytic degradation of methylene blue on PbO2-ZrO2 nanocomposite electrodes prepared by pulse electrodeposition, J Hazard Mater 263 Pt 2 (2013) 726-34. https://doi.org/10.1016/j.jhazmat.2013.10.038.
[44] L. He, L.F. Dumée, C. Feng, L. Velleman, R. Reis, F. She, W. Gao, L. Kong, Promoted water transport across graphene oxide–poly(amide) thin film composite membranes and their antibacterial activity, Desalination 365 (2015) 126-135. https://doi.org/10.1016/j.desal.2015.02.032.
[45] N.F. Che Lah, A.L. Ahmad, M.H. Mohd Amri, J.Y. Chin, Configuration of molecularly imprinted polymers for specific uptake of pharmaceutical in aqueous media through radical polymerization method, Journal of Polymer Research 29(2) (2022). https://doi.org/10.1007/s10965-022-02908-8.
[46] C. Gumeci, D. Do, S.C. Barton, Electrospun Carbon Nanofibers as Supports for Bioelectrodes, Electrocatalysis 8(4) (2017) 321-328. https://doi.org/10.1007/s12678-017-0373-y.
[47] M. Faccini, G. Borja, M. Boerrigter, D. Morillo Martín, S. Martìnez Crespiera, S. Vázquez-Campos, L. Aubouy, D. Amantia, Electrospun Carbon Nanofiber Membranes for Filtration of Nanoparticles from Water, Journal of Nanomaterials 2015 (2015) 1-9. https://doi.org/10.1155/2015/247471.
[48] W. Liu, G. Walker, S. Price, X. Yang, J. Li, C. Bunt, Electrospun Membranes as a Porous Barrier for Molecular Transport: Membrane Characterization and Release Assessment, Pharmaceutics 13(6) (2021). https://doi.org/10.3390/pharmaceutics13060916.
[49] R. Bagherzadeh, S.S. Najar, M. Latifi, M.A. Tehran, L. Kong, A theoretical analysis and prediction of pore size and pore size distribution in electrospun multilayer nanofibrous materials, J Biomed Mater Res A 101(7) (2013) 2107-17. https://doi.org/10.1002/jbm.a.34487.
[50] J.L. Lowery, N. Datta, G.C. Rutledge, Effect of fiber diameter, pore size and seeding method on growth of human dermal fibroblasts in electrospun poly(epsilon-caprolactone) fibrous mats, Biomaterials 31(3) (2010) 491-504. https://doi.org/10.1016/j.biomaterials.2009.09.072.
[51] H. Ahn, S.Y. Yeo, B.S. Lee, Designing Materials and Processes for Strong Polyacrylonitrile Precursor Fibers, Polymers (Basel) 13(17) (2021). https://doi.org/10.3390/polym13172863.
[52] Z. Li, O. Zabihi, J. Wang, Q. Li, J. Wang, W. Lei, M. Naebe, Hydrophilic PAN based carbon nanofibres with improved graphitic structure and enhanced mechanical performance using ethylenediamine functionalized graphene, RSC Advances 7(5) (2017) 2621-2628. https://doi.org/10.1039/c6ra24719a.

[53] K. Ma, P. Chen, B. Wang, G. Cui, X. Xu, A study of the effect of oxygen plasma treatment on the interfacial properties of carbon fiber/epoxy composites, Journal of Applied Polymer Science (2010) n/a-n/a. https://doi.org/10.1002/app.32549.
[54] O.-K. Park, W. Young Kim, S. Min Kim, N.-H. You, Y. Jeong, H. Su Lee, B.-C. Ku, Effect of oxygen plasma treatment on the mechanical properties of carbon nanotube fibers, Materials Letters 156 (2015) 17-20. https://doi.org/10.1016/j.matlet.2015.04.141.
[55] C.-C. Lai, C.-T. Lo, Plasma oxidation of electrospun carbon nanofibers as supercapacitor electrodes, RSC Advances 5(49) (2015) 38868-38872. https://doi.org/10.1039/c5ra04284d.
[56] E. Ortiz-Ortega, S. Hosseini, S.O. Martinez-Chapa, M.J. Madou, Aging of plasma-activated carbon surfaces: Challenges and opportunities, Applied Surface Science 565 (2021). https://doi.org/10.1016/j.apsusc.2021.150362.
[57] J. Rao, L. Bao, B. Wang, M. Fan, L. Feo, Plasma surface modification and bonding enhancement for bamboo composites, Composites Part B: Engineering 138 (2018) 157-167. https://doi.org/10.1016/j.compositesb.2017.11.025.
[58] H. Tang, W. Chen, J. Wang, T. Dugger, L. Cruz, D. Kisailus, Electrocatalytic N-Doped Graphitic Nanofiber - Metal/Metal Oxide Nanoparticle Composites, Small 14(11) (2018) e1703459. https://doi.org/10.1002/smll.201703459.
[59] F.G. Pacheco, A.A.C. Cotta, H.F. Gorgulho, A.P. Santos, W.A.A. Macedo, C.A. Furtado, Comparative temporal analysis of multiwalled carbon nanotube oxidation reactions: Evaluating chemical modifications on true nanotube surface, Applied Surface Science 357 (2015) 1015-1023. https://doi.org/10.1016/j.apsusc.2015.09.054.
[60] Y. Bao, Y.S. Tay, T.-T. Lim, R. Wang, R.D. Webster, X. Hu, Polyacrylonitrile (PAN)-induced carbon membrane with in-situ encapsulated cobalt crystal for hybrid peroxymonosulfate oxidation-filtration process: Preparation, characterization and performance evaluation, Chemical Engineering Journal 373 (2019) 425-436. https://doi.org/10.1016/j.cej.2019.05.058.
[61] Y. Zhang, Q. Su, W. Xu, G. Cao, Y. Wang, A. Pan, S. Liang, A Confined Replacement Synthesis of Bismuth Nanodots in MOF Derived Carbon Arrays as Binder-Free Anodes for Sodium-Ion Batteries, Adv Sci (Weinh) 6(16) (2019) 1900162. https://doi.org/10.1002/advs.201900162.
[62] A. Ganguly, S. Sharma, P. Papakonstantinou, J. Hamilton, Probing the Thermal Deoxygenation of Graphene Oxide Using High-Resolution In Situ X-ray-Based Spectroscopies, The Journal of Physical Chemistry C 115(34) (2011) 17009-17019. https://doi.org/10.1021/jp203741y.
[63] F.M. El-Hossary, A. Ghitas, A.M.A. El-Rahman, A.A. Ebnalwaled, M.A. Shahat, M.H. Fawey, Cold RF oxygen plasma treatment of graphene oxide films, Journal of Materials Science: Materials in Electronics 32(12) (2021) 15718-15731. https://doi.org/10.1007/s10854-021-06123-x.
[64] J. Chen, J. Pei, H. Zhao, Effect of Oxygen Plasma Treatment on the Structure and Mechanical Properties of Bilayer Graphene Studied by Molecular Dynamics Simulation, The Journal of Physical Chemistry C 125(35) (2021) 19345-19352. https://doi.org/10.1021/acs.jpcc.1c02610.
[65] M.B. Taskin, T. Ahmad, L. Wistlich, L. Meinel, M. Schmitz, A. Rossi, J. Groll, Bioactive Electrospun Fibers: Fabrication Strategies and a Critical Review of Surface-Sensitive Characterization and Quantification, Chem Rev 121(18) (2021) 11194-11237. https://doi.org/10.1021/acs.chemrev.0c00816.

[66] A. Bismarck, M.E. Kumru, J. Springer, Influence of Oxygen Plasma Treatment of PAN-Based Carbon Fibers on Their Electrokinetic and Wetting Properties, Journal of Colloid and Interface Science 210(1) (1999) 60-72. https://doi.org/10.1006/jcis.1998.5912.
[67] B.M. Thamer, A. Aldalbahi, A.M. Moydeen, A.M. Al-Enizi, H. El-Hamshary, M.H. El-Newehy, Fabrication of functionalized electrospun carbon nanofibers for enhancing lead-ion adsorption from aqueous solutions, Sci Rep 9(1) (2019) 19467. https://doi.org/10.1038/s41598-019-55679-6.
[68] H.A. Bland, E.L.H. Thomas, G.M. Klemencic, S. Mandal, D.J. Morgan, A. Papageorgiou, T.G. Jones, O.A. Williams, Superconducting Diamond on Silicon Nitride for Device Applications, Sci Rep 9(1) (2019) 2911. https://doi.org/10.1038/s41598-019-39707-z.
[69] P. Innocenzi, L. Stagi, Carbon-based antiviral nanomaterials: graphene, C-dots, and fullerenes. A perspective, Chem Sci 11(26) (2020) 6606-6622. https://doi.org/10.1039/d0sc02658a.
[70] S.C. Smith, D.F. Rodrigues, Carbon-based nanomaterials for removal of chemical and biological contaminants from water: A review of mechanisms and applications, Carbon 91 (2015) 122-143. https://doi.org/10.1016/j.carbon.2015.04.043.
[71] Z. Wang, M. Elimelech, S. Lin, Environmental Applications of Interfacial Materials with Special Wettability, Environ Sci Technol 50(5) (2016) 2132-50. https://doi.org/10.1021/acs.est.5b04351.
[72] M. Tang, L. Zheng, D. Hou, X. Jia, J. Wang, Microstructure design and construction of anti-wetting and anti-fouling multifunctional Janus membrane for robust membrane distillation, Chemical Engineering Journal 430 (2022). https://doi.org/10.1016/j.cej.2021.132973.
[73] M.-G. Yan, L.-Q. Liu, Z.-Q. Tang, L. Huang, W. Li, J. Zhou, J.-S. Gu, X.-W. Wei, H.-Y. Yu, Plasma surface modification of polypropylene microfiltration membranes and fouling by BSA dispersion, Chemical Engineering Journal 145(2) (2008) 218-224. https://doi.org/10.1016/j.cej.2008.04.007.
[74] P. Slepička, K. Setničková, Z. Petrusová, N. Slepičková Kasálková, Z. Kolská, J. Siegel, J.C. Jansen, E. Esposito, A. Fuoco, V. Švorčík, P. Izák, The influence of surface treatment and activation of thin film composite membranes with plasma discharge and determination of their physicochemical properties, Separation and Purification Technology 220 (2019) 52-60. https://doi.org/10.1016/j.seppur.2019.03.050.
[75] K. Huang, A. Hu, C. Huang, Y. Li, H. Zhou, Y. Xu, Q. Tang, S. Zhou, C. Chen, X. Chen, Ultrafast Activating Strategy to Significantly Enhance the Electrocatalysis of Commercial Carbon Cloth for Oxygen Evolution Reaction and Overall Water Splitting, ChemNanoMat 6(4) (2020) 542-549. https://doi.org/10.1002/cnma.202000017.
[76] F. Zhang, G. Song, D. Gandla, Y. Ein-Eli, D.Q. Tan, Synergy of Oxygen Plasma and Al2O3 Atomic Layer Deposition on Improved Electrochemical Stability of Activated Carbon-Based Supercapacitor, Frontiers in Energy Research 9 (2021). https://doi.org/10.3389/fenrg.2021.653203.
[77] Y. Juang, E. Nurhayati, C. Huang, J.R. Pan, S. Huang, A hybrid electrochemical advanced oxidation/microfiltration system using BDD/Ti anode for acid yellow 36 dye wastewater treatment, Separation and Purification Technology 120 (2013) 289-295. https://doi.org/10.1016/j.seppur.2013.09.042.
[78] Q. Li, Q. Zhang, H. Cui, L. Ding, Z. Wei, J. Zhai, Fabrication of cerium-doped lead dioxide anode with improved electrocatalytic activity and its application for removal of Rhodamine B, Chemical Engineering Journal 228 (2013) 806-814. https://doi.org/10.1016/j.cej.2013.05.064.

[79] S. Adhikari, Y. Kwon, D.-H. Kim, Three-dimensional core–shell structured NiCo2O4@CoS/Ni-Foam electrocatalyst for oxygen evolution reaction and electrocatalytic oxidation of urea, Chemical Engineering Journal 402 (2020). https://doi.org/10.1016/j.cej.2020.126192.
[80] S. Chen, S. Zhang, M. Galluzzi, F. Li, X. Zhang, X. Yang, X. Liu, X. Cai, X. Zhu, B. Du, J. Li, P. Huang, Insight into multifunctional polyester fabrics finished by one-step eco-friendly strategy, Chemical Engineering Journal 358 (2019) 634-642. https://doi.org/10.1016/j.cej.2018.10.070.
[81] W. Zhai, H. Yu, H. Chen, L. Li, D. Li, Y. Zhang, T. He, Stable fouling resistance of polyethylene (PE) separator membrane via oxygen plasma plus zwitterion grafting, Separation and Purification Technology 293 (2022). https://doi.org/10.1016/j.seppur.2022.121091.
[82] Z. He, Y. Lv, T. Zhang, Y. Zhu, L. Dai, S. Yao, W. Zhu, L. Wang, Electrode materials for vanadium redox flow batteries: Intrinsic treatment and introducing catalyst, Chemical Engineering Journal 427 (2022). https://doi.org/10.1016/j.cej.2021.131680.
[83] Y. Wang, J. Zhu, H. Huang, H.-H. Cho, Carbon nanotube composite membranes for microfiltration of pharmaceuticals and personal care products: Capabilities and potential mechanisms, Journal of Membrane Science 479 (2015) 165-174. https://doi.org/10.1016/j.memsci.2015.01.034.
[84] R. Lyubimenko, D. Busko, B.S. Richards, A.I. Schafer, A. Turshatov, Efficient Photocatalytic Removal of Methylene Blue Using a Metalloporphyrin-Poly(vinylidene fluoride) Hybrid Membrane in a Flow-Through Reactor, ACS Appl Mater Interfaces 11(35) (2019) 31763-31776. https://doi.org/10.1021/acsami.9b04601.
[85] A.O. Rashed, A.M.K. Esawi, A.R. Ramadan, Novel Polysulfone/Carbon Nanotube-Polyamide Thin Film Nanocomposite Membranes with Improved Water Flux for Forward Osmosis Desalination, ACS Omega 5(24) (2020) 14427-14436. https://doi.org/10.1021/acsomega.0c00973.
[86] L. Zheng, Y. Su, L. Wang, Z. Jiang, Adsorption and recovery of methylene blue from aqueous solution through ultrafiltration technique, Separation and Purification Technology 68(2) (2009) 244-249. https://doi.org/10.1016/j.seppur.2009.05.010.
[87] D.T. Nguyen, H.N. Tran, R.-S. Juang, N.D. Dat, F. Tomul, A. Ivanets, S.H. Woo, A. Hosseini-Bandegharaei, V.P. Nguyen, H.-P. Chao, Adsorption process and mechanism of acetaminophen onto commercial activated carbon, Journal of Environmental Chemical Engineering 8(6) (2020). https://doi.org/10.1016/j.jece.2020.104408.
[88] A.O. Rashed, A. Merenda, T. Kondo, M. Lima, J. Razal, L. Kong, C. Huynh, L.F. Dumée, Carbon nanotube membranes – Strategies and challenges towards scalable manufacturing and practical separation applications, Separation and Purification Technology 257 (2021). https://doi.org/10.1016/j.seppur.2020.117929.
[89] P.T. Lan Huong, N. Tu, H. Lan, L.H. Thang, N. Van Quy, P.A. Tuan, N.X. Dinh, V.N. Phan, A.T. Le, Functional manganese ferrite/graphene oxide nanocomposites: effects of graphene oxide on the adsorption mechanisms of organic MB dye and inorganic As(v) ions from aqueous solution, RSC Adv 8(22) (2018) 12376-12389. https://doi.org/10.1039/c8ra00270c.
[90] N. Mohammad, Y. Atassi, Adsorption of methylene blue onto electrospun nanofibrous membranes of polylactic acid and polyacrylonitrile coated with chloride doped polyaniline, Sci Rep 10(1) (2020) 13412. https://doi.org/10.1038/s41598-020-69825-y.

[91] V. Bernal, A. Erto, L. Giraldo, J.C. Moreno-Pirajan, Effect of Solution pH on the Adsorption of Paracetamol on Chemically Modified Activated Carbons, Molecules 22(7) (2017). https://doi.org/10.3390/molecules22071032.
[92] S.W. Nam, D.J. Choi, S.K. Kim, N. Her, K.D. Zoh, Adsorption characteristics of selected hydrophilic and hydrophobic micropollutants in water using activated carbon, J Hazard Mater 270 (2014) 144-52. https://doi.org/10.1016/j.jhazmat.2014.01.037.
[93] R. Reis, L.F. Dumée, A. Merenda, J.D. Orbell, J.A. Schütz, M.C. Duke, Plasma-induced physicochemical effects on a poly(amide) thin-film composite membrane, Desalination 403 (2017) 3-11. https://doi.org/10.1016/j.desal.2016.06.009.
[94] R. Reis, M. Duke, A. Merenda, B. Winther-Jensen, L. Puskar, M.J. Tobin, J.D. Orbell, L.F. Dumée, Customizing the surface charge of thin-film composite membranes by surface plasma thin film polymerization, Journal of Membrane Science 537 (2017) 1-10. https://doi.org/10.1016/j.memsci.2017.05.013.
[95] T. Mei, M. Gao, D. Liu, Y. Wang, Y. Huang, Enhanced electrocatalytic activity of carbon cloth by synergetic effect of plasma and acid treatment, Plasma Science and Technology 23(2) (2021). https://doi.org/10.1088/2058-6272/abd8b4.
[96] I. Kondratowicz, M. Nadolska, S. Şahin, M. Łapiński, M. Prześniak-Welenc, M. Sawczak, E.H. Yu, W. Sadowski, K. Żelechowska, Tailoring properties of reduced graphene oxide by oxygen plasma treatment, Applied Surface Science 440 (2018) 651-659. https://doi.org/10.1016/j.apsusc.2018.01.168.
[97] L. Lin, H. Wang, H. Luo, P. Xu, Enhanced photocatalysis using side-glowing optical fibers coated with Fe-doped TiO2 nanocomposite thin films, Journal of Photochemistry and Photobiology A: Chemistry 307-308 (2015) 88-98. https://doi.org/10.1016/j.jphotochem.2015.04.010.
[98] S. Raha, D. Mohanta, M. Ahmaruzzaman, Novel CuO/Mn3O4/ZnO nanocomposite with superior photocatalytic activity for removal of Rabeprazole from water, Sci Rep 11(1) (2021) 15187. https://doi.org/10.1038/s41598-021-94066-y.
[99] L. Zhao, X. Zhang, Z. Liu, C. Deng, H. Xu, Y. Wang, M. Zhu, Carbon nanotube-based electrocatalytic filtration membrane for continuous degradation of flow-through Bisphenol A, Separation and Purification Technology 265 (2021). https://doi.org/10.1016/j.seppur.2021.118503.
[100] F.K. Malekabadi, F. Yousefi, R. Karimi, M. Ghaedi, K. Dashtian, Electrocatalytic membrane containing CuFeO2/nanoporous carbon for organic dye removal application, Chemical Engineering Research and Design 183 (2022) 345-356. https://doi.org/10.1016/j.cherd.2022.05.019.
[101] A. Xue, Z.W. Yuan, Y. Sun, A.Y. Cao, H.Z. Zhao, Electro-oxidation of perfluorooctanoic acid by carbon nanotube sponge anode and the mechanism, Chemosphere 141 (2015) 120-6. https://doi.org/10.1016/j.chemosphere.2015.06.095.
[102] J. Zhou, Y. Zhang, M. Balda, V. Presser, F.-D. Kopinke, A. Georgi, Electro-assisted removal of polar and ionic organic compounds from water using activated carbon felts, Chemical Engineering Journal 433 (2022). https://doi.org/10.1016/j.cej.2021.133544.
[103] M. Coha, G. Farinelli, A. Tiraferri, M. Minella, D. Vione, Advanced oxidation processes in the removal of organic substances from produced water: Potential, configurations, and research needs, Chemical Engineering Journal 414 (2021). https://doi.org/10.1016/j.cej.2021.128668.
[104] G. Chen, Electrochemical technologies in wastewater treatment, Separation and Purification Technology 38(1) (2004) 11-41. https://doi.org/10.1016/j.seppur.2003.10.006.

[105] N. Li, S. Dong, W. Lv, S. Huang, H. Chen, Y. Yao, W. Chen, Enhanced electrocatalytic oxidation of dyes in aqueous solution using cobalt phthalocyanine modified activated carbon fiber anode, Science China Chemistry 56(12) (2013) 1757-1764. https://doi.org/10.1007/s11426-013-4942-5.
[106] M. Liu, H. Xia, W. Lu, T. Xu, Z. Zhu, W. Chen, Electrocatalytic degradation of organic contaminants using carbon fiber coupled with cobalt phthalocyanine electrode, Journal of Applied Electrochemistry 46(5) (2016) 583-592. https://doi.org/10.1007/s10800-016-0939-z.
[107] C.A. Martínez-Huitle, S. Ferro, Electrochemical oxidation of organic pollutants for the wastewater treatment: direct and indirect processes, Chemical Society Reviews 35(12) (2006) 1324-1340. https://doi.org/10.1039/B517632H.
[108] K. Liu, J.C. Yu, H. Dong, J.C.S. Wu, M.R. Hoffmann, Degradation and Mineralization of Carbamazepine Using an Electro-Fenton Reaction Catalyzed by Magnetite Nanoparticles Fixed on an Electrocatalytic Carbon Fiber Textile Cathode, Environ Sci Technol 52(21) (2018) 12667-12674. https://doi.org/10.1021/acs.est.8b03916.
[109] L.A. Pereira, D.A. de Lima Almeida, A.B. Couto, N.G. Ferreira, Titanium dioxide/oxidized carbon fiber electrodes electrochemically produced and their influences on Brilliant Green dye degradation, Materials Research Bulletin 122 (2020). https://doi.org/10.1016/j.materresbull.2019.110642.
[110] N.H. Luan, Y.-T. Yang, C.-F. Chang, Electrochemical degradation of methylene blue accompanied with the reduction of CO2 by using carbon nanotubes grown on carbon fiber electrodes, Sustainable Environment Research 32(1) (2022). https://doi.org/10.1186/s42834-022-00122-1.